Journal of Hydroscience and Hydraulic Engineering
Vol. 19, No.1 May, 2001, 153-162

Effect of Diurnal Inequalities on Vertical Mixing in Estuary

By

Makoto Ifuku

and

Toshiyuki Haramaki

Department of Civil and Environmental Engineering
Ehime University, Matsuyama, Ehime 790-8577, Japan

SYNOPSIS

The effects of diurnal inequality and river discharge rates on the mixing of density currents in an estuary are investigated. Numerical results obtained with a new two-dimensional numerical model is developed.match closely with observed results in the higher isohalines, but differ greatly in the lower isohalines. The effects of the diurnal inequality on saline intrusion can be classified into two patterns that are explainable by a new parameter defined in terms of the tidal amplitude. When the river discharge rate exceeds 1,000 m^3/s, the intrusion of salt water almost completely stops.

INTRODUCTION

In recent years, a combination of unusual weather, increased water demand water, decreasing water levels, and dredging has caused saline water to intrude upstream into rivers. This poses a serious problem for river environments. There is a need to clarify the mixing process of density currents and the temporal and spatial non-uniformities in tidal estuaries. Investigation of these phenomena will clarify not only the intrusion mechanism but also the diffusion and circulation of pollutant water and the transport of bed materials by gravitational circulation and turbulence.

Since flows in an estuary are dependent on estuary geometry, complicated flow patterns induced by the features of a particular estuary are found.

In numerical models for the prediction of saline water behavior, it is necessary to consider tidal level changes at the seaward boundary as a sinusoidal wave that ignores diurnal inequalities. Partially mixed and well-mixed patterns can be observed during changes in the estuary's tidal range.

Assumption, however, of tidal level change being sinusoidal would provide in accurate results in describing true behaviors of density current in the river.

Field measurements were carried out by the first author at the Hiji river in Ehime Prefecture, Japan in 1978. The results were used to develop a two-dimensional numerical model that could predict density current fields. The investigation also analyzed the effects of river discharge rates and diurnal inequality on density current field in Hiji river in Ehime Prefecture, Japan.

NUMERICAL ANALYSIS

Governing Equations

Flow

After integrating over channel width and using a shallow water approximation, the formulation for

a vertical two-dimensional density current is as follows:

The conservation of longitudinal momentum leads to

$$\frac{\partial u}{\partial t}+\frac{1}{B}\frac{\partial}{\partial x}(Bu^2)+\frac{\partial}{\partial z}(uw)=-\frac{1}{\rho_0}\frac{\partial p}{\partial x}+\frac{1}{\rho_0}\frac{1}{B}\frac{\partial}{\partial x}(B\tau_{xx})+\frac{1}{\rho_0}\frac{\partial \tau_{xz}}{\partial z} \tag{1}$$

where t = time; x = longitudinal coordinate (positive upstream); z = vertical coordinate (positive upward); u, w = longitudinal and vertical velocities, respectively; ρ = density; ρ_0 = reference density; p = pressure; and B = channel width, which is assumed to be dependent only on x.

Moreover, τ_{xx} and τ_{zx} are the Reynolds stresses and are described in the notation of Cartesian tensors as follows:

$$\left.\begin{aligned}\tau_{ji}/\rho_0&=(\nu+\nu_t)\left(\frac{\partial u_i}{\partial x_j}+\frac{\partial u_j}{\partial x_i}\right)\\ \nu_t&=(c_s\Delta)^2\left[\left(\frac{\partial u_i}{\partial x_j}+\frac{\partial u_j}{\partial x_i}\right)\frac{\partial u_i}{\partial x_j}\right]^{1/2}\end{aligned}\right\} \tag{2}$$

where ν = kinematic viscosity; ν_t = SGS (subgrid-scale) diffusivity suggested by Smagorinsky(5); c_s = Smagorinsky constant; and $\Delta=(\Delta x\Delta z)^{1/3}$(with Δx and Δz the londitudinal and vertical grid intervals, respectively).

Using a shallow water approximation, the conservation of vertical momentum is reduced to the hydrostatic pressure distribution:

$$\frac{\partial p}{\partial z}=-\rho g \tag{3}$$

where g = gravitational acceleration. Integration of eq.(3) with respect to z yields an equation for pressure as

$$\left.\begin{aligned}p&=\rho_0 g(\xi-z)+\beta g\int_{z_b}^{\xi}S\,dz\\ \beta&=\rho_0(\rho_s-\rho_0)/\rho_s\end{aligned}\right\} \tag{4}$$

where ξ = position of the free water surface; z_b = z-coordinate of the bottom; ρ_s = density of salt water; and S = salinity.

The continuity equation leads to

$$\frac{1}{B}\frac{\partial(Bu)}{\partial x}+\frac{\partial w}{\partial z}=0 \tag{5}$$

Integration of eq.(5) over water depth and substituting the kinematic boundary condition, yields

$$\frac{\partial \xi}{\partial t}+\frac{1}{B}\frac{\partial}{\partial x}\left(B\int_{z_b}^{\xi}u\,dz\right)=0 \tag{6}$$

Salt Content

The equation of conservation of salt content leads to

$$\frac{\partial S}{\partial t}+\frac{1}{B}\frac{\partial}{\partial x}(BuS)+\frac{\partial}{\partial z}(wS)=\frac{1}{B}\frac{\partial}{\partial x}\left(BK_{xx}\frac{\partial S}{\partial x}\right)+\frac{\partial}{\partial z}\left(K_{zz}\frac{\partial S}{\partial z}\right) \tag{7}$$

where K_{xx}, K_{zz} = turbulent diffusivities.

The equation for state is as follows:

$$\rho=\rho_0+\beta S \tag{8}$$

The turbulent diffusivities, K_{xx} and K_{zz}, are assumed to be as follows (refer to Bear (1)):

$$\left.\begin{aligned}K_{xx}&=\gamma_x(a_L u^2+a_T w^2)/q\\ K_{zz}&=\gamma_z(a_T u^2+a_L w^2)/q\\ q&=(u^2+w^2)^{1/2}\end{aligned}\right\} \tag{9}$$

where γ_x, γ_z = constants of proportionality; and a_T, a_L=characteristic lengths, defined as follows.

$$a_T = \Delta\ ,\ a_L = c_1 \cdot a_T \tag{10}$$

where c_1 = empirical constant.

Boundary Conditions

The mathematical model requires boundary conditions and initial conditions with respect both to tidal motion and salinity. Designation of the model as either descriptive or predictive depends on how the vertical momentum and mass exchange are formulated, and how the boundary conditions are treated.

Free Surface Boundary

At the water surface $z = \xi$, the conditions are:

$$\left.\begin{aligned} &\partial u/\partial z = 0 \\ &w_\xi = \partial\xi/\partial t + u_\xi(\partial\xi/\partial x) \\ &w_\xi S - K_{zz}(\partial S/\partial z) = 0 \end{aligned}\right\} \tag{11}$$

where u_ξ, w_ξ = horizontal and vertical velocities of fluid particles at the water surface, respectively.

Bottom Boundary

At the bottom $z = z_b$, the conditions are:

$$\left.\begin{aligned} &u = 0,\ \ w = 0 \ \ \text{(nonslip)} \\ &\partial S/\partial z = 0 \end{aligned}\right\} \tag{12}$$

Boundary at River Mouth

At the river mouth, the surface elevation, η, and the water level, ξ, must be identified as

$$\left.\begin{aligned} &\eta(t) = a\sin\sigma t \\ &\xi(t) = h + \eta(t) \end{aligned}\right\} \tag{13}$$

where h = mean water depth; a= tidal amplitude; σ = angular frequency ($\sigma = 2\pi/T$; T : the tidal period). Further, a boundary condition for longitudinal velocity is required. Because no velocity profiles at the river mouth are generally available during the tidal cycle, a through-flow condition is imposed:

$$\partial^2 u/\partial x^2 = 0 \tag{14}$$

Finally, a condition for the conservation of salinity must be given. During a flood tide, the increase in concentration is dependent both on t and z. During an ebb tide, a condition is set in a similar way to the condition for longitudinal velocity.

$$\left.\begin{aligned} &S = S_0\, G(z,t) \quad u(z) \geq 0 \\ &G(z,t) \equiv (1 - S') + S'\sin\sigma t \quad \text{(without diurnal inequality)} \\ &G(z,t) \equiv 1 - (1 - \eta/\eta_{max})S' \quad \text{(with diurnal inequality)} \\ &\partial^2 S/\partial x^2 = 0 \quad u(z) < 0 \end{aligned}\right\} \tag{15}$$

where S_0 = salinity of the sea; S' = a weighting coefficient and η_{max} = the maximum tidal elevation. A functional form of $G(z,t)$ is one of the points to be discussed in this paper. As the first assumption, a piece-wise linearized function of t, independent of z, is applied.

Upstream Boundary

Once the river discharge is given, the velocity profile in the river channel course is assumed to be logarithmic.

$$\left.\begin{aligned} &u = u_\xi[\ln\{\tfrac{(e-1)}{(\xi - z_b)}(z - z_b) + 1\}] \\ &\partial^2 S/\partial x^2 = 0 \end{aligned}\right\} \tag{16}$$

Coordinate Transformation

In the physical domain, the water surface is a moving boundary because of tides, and the bottom topography also changes in space. Furthermore, the longitudinal area of interest is not always rectangular because of variations in the bottom and the free surface. To obtain a good representation of flow, accurate descriptions of free surface and bottom profiles are necessary. For a numerical approach based on finite differences, however, a rectangular grid that is coincident with the boundaries is recommended. Therefore, the test section is modified by a simple transformation into a rectangle. This coordinate transformation is applied to the governing equations, and the spatial and temporal behaviors of flow and salinity are described in detail by Ifuku and Kusu(3).

Numerical Results

Analysis based on Experiment by Perrels and Karelse(4)

The results of a flume test conducted by Perrels and Kareles were used to verify the numerical model. It is assumed that the density difference between river water and seawater, $\Delta\rho(\Delta\rho = \rho_s - \rho_0)$, is 23.8 kg/m^3. At the downstream boundary, the surface elevation is computed using Airy wave theory with a wave amplitude of 2.5 cm and a period of 558.7 s. The river discharge at the upstream boundary is set to 2.9x10^{-3} m^3/s. The length, width, and depth of the channel are 101.5 m, 0.672 m, and 0.216 m, respectively. A nonslip condition is applied at the bottom. The horizontal grid size is 0.915 m and the water depth is divided into 20 layers. The numerical time step is $T/2000$. The Smagorinsky constant in eq.(2) is set to 0.1 or 0.2.

Vertical Profile of Horizontal Velocity

Figure 1(a) shows a vertical profile at point $x = 7.32$ m during the slack phase of an ebb tide (referred to as M.E.V.). For a Smagorinsky constant of 0.1, the simulated velocity is slightly larger than the experimental value from the bottom to a height equivalent to one-fifth of the water depth. The simulated results agree well with the experimental ones, even at intermediate depths. Overall, the difference between experimental and simulated results is very small. When the Smagorinsky constant is set to 0.2, the simulated results are slightly larger than the experimental ones at intermediate depths. Further, the simulated results underestimate the experimental ones near the free surface.

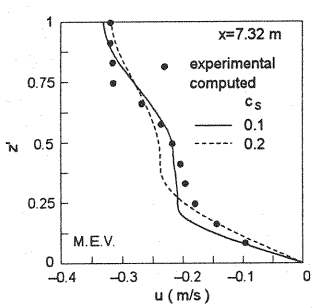

(a)M.E.V.

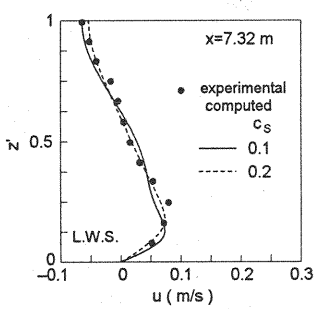

(b)L.W.S.

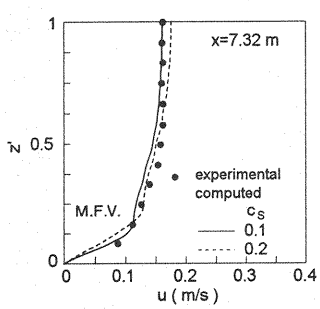

(a)M.F.V.

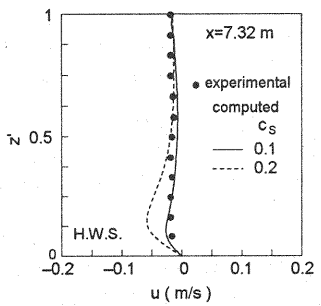

(b)H.W.S.

Figure 1 Profile of longitudinal velocity

Figure 1(b) shows a vertical profile at point $x = 7.32$ m at low water (referred to as L.W.S.). Whatever the Smagorinsky constant, the profiles of simulated values are similar to each other and the simulated values agree well with the experimental values throughout the water column.

Figure 1(c) shows a vertical profile at point $x = 7.32$ m during the slack phase of a flood tide (referred to as M.F.V.). For a Smagorinsky constant of 0.1, the simulated velocity is slightly smaller than the experimental value at intermediate depths. However, the difference is very small. The simulated values agree very well with the experimental values near the free surface and the bottom. For a Smagorinsky constant of 0.2, the simulated results are lower than the experimental values near the bottom and larger than the experimental values near the free surface.

Figure 1(d) shows the vertical distribution at point $x = 7.32$ m at high water (referred to as H.W.S.). For a Smagorinsky constant of 0.1, the simulated velocity agrees well with the experimental value. Meanwhile, when the Smagorinsky constant is set to 0.2, the simulated velocity agrees well with the experimental value from intermediate depths up to the water surface. However, the simulated value is approximately three times the experimental value near the bottom.

In previous work by the first author, agreement between experimental and simulated values for velocity profile was found to be highly satisfactory in cases of a neutral stratification and a Smagorinsky constant of 0.1.

Judging from these results, the flow structure of density-stratified flow can be represented by a SGS-eddy viscosity. Also, it is appropriate to set the Smagorinsky constant to 0.1. Thus the Smagorinsky constant is fixed at 0.1 hereafter.

Analysis based on the Observations of the Hiji river

According to the Hiji river service map, the upstream extent of saline water intrusion is about 9 km from the river mouth. Therefore, the simulation covers a region extending 10.5 km upstream from the river mouth. The sea boundary is placed 500 m offshore. Figure 2 shows the profile of river width as used for simulation. Near the river mouth, a sand bar has formed and the river narrows. Finally, the 1978 riverbed profile is used for the simulation. The observed data were collected by the first author on September 14, October 24, and November 29, 1978.

Spatial Distribution of Velocity

Figure 3 shows the temporal variation of tidal displacement on September 14, 1978. The diurnal inequality is significant. Further, river discharge at the Goro observatory, which is about 11 km from the river mouth, was approximately 9-10 m^3/s during the period September 8-14, 1978.

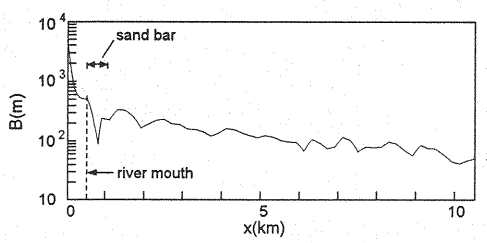

Figure 2 River width

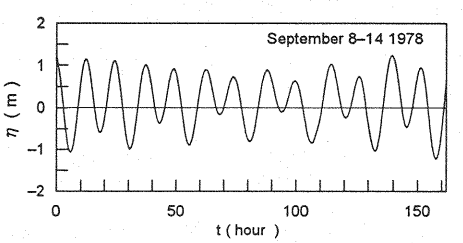

Figure 3 Tidal displacement

Figure 4 shows the spatial distribution of velocity for two phases on September 14, 1978. Figure 4(a) shows the simulated results for the slack phase of the ebb tide. With decreasing tidal level and the beginning of fresh water flow downstream, the direction was turned downstream and the counterclockwise circulation pattern developed at x=3 and 6 km near the bottom.

Figure 4(b) shows the results for the slack phase of the flood tide. With increasing tidal level and saline water intrusion, the direction is turned upstream from the river mouth to x=8 km. However, as the shoal is about x=9.5 km, the downstream velocity increases near the shoal.

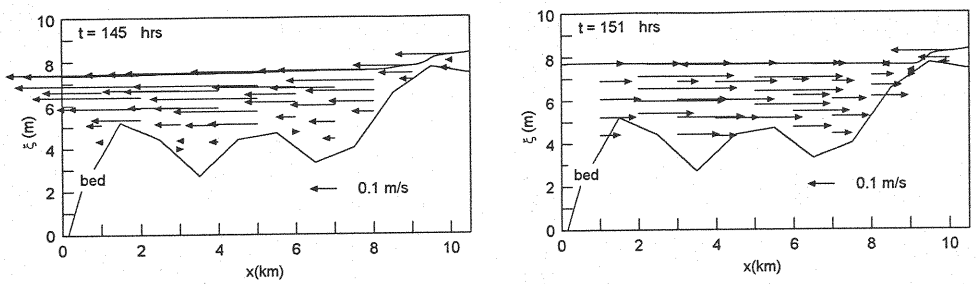

(a)slack in flood (b)slack in ebb

Figure 4 Spatial distribution of velocity

Spatial Distribution of Salinity

Figure 5 shows the spatial distribution of isohalines at three representative phases. The filled circles, squares, diamonds, and triangles are the corresponding observed values, S/S_0 are 0.025, 0.05, 0.25 and 0.5, respectively and the solid lines are the simulated values.

Figure 5(a) gives the results for the high water phase on September 14, 1978. Salt water intrudes upstream induced by the density difference between fresh and salt waters.

Figure 5(b) gives the results for the low water phase. With decreasing tidal level, the salt water retreats downstream. This backwash of salt water is sluggish near the bottom, as a consequence of bottom topography. As a result, relatively salty water was trapped within the basins between x=5.5 to 7 km.

Figure 5(c) gives the results for the slack phase of the flood tide. The salt water intrudes upstream with increasing the tidal level. At the same time, the trapped salty water within the basins is reduced and the salinity gradient rises. These results suggest that as the downstream velocity increases near the shoal at x=9.5 km, it prevents a long intrusion of saline water. The 9.5 km point approximately corresponds to the upstream extent of saline water intrusion.

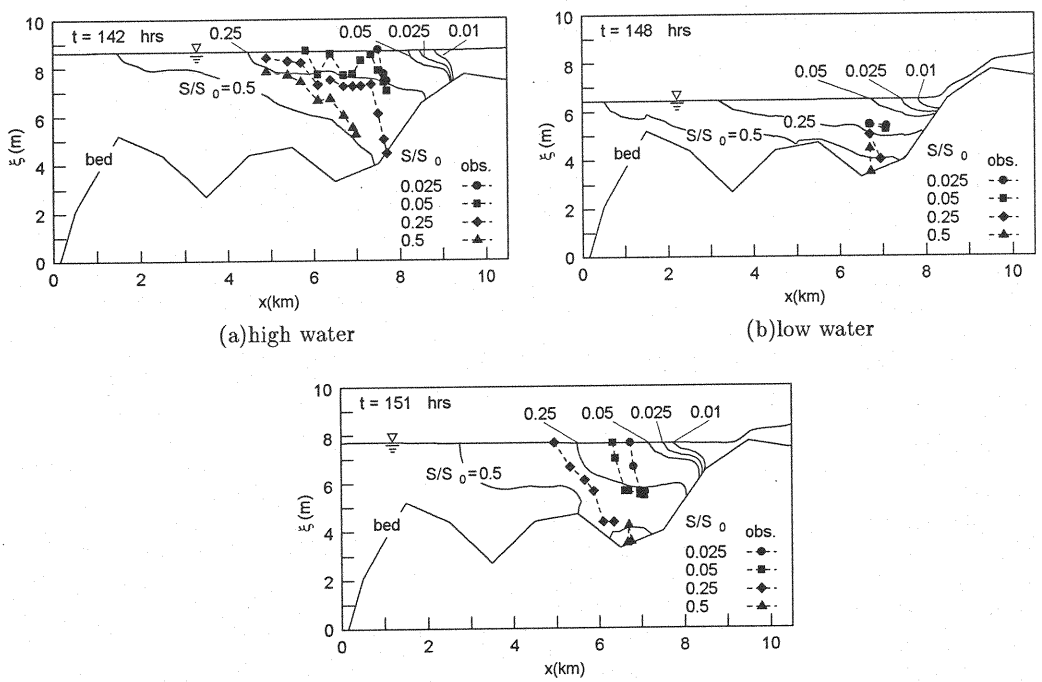

(a)high water (b)low water

(c)slack at flood tide

Figure 5 Isohalines (September 14, 1978)

It is not yet possible to conclude that the present simulation models the observed phenomena well. We still have to consider a number of processes, including (i) local changes in water depth at the site, which are disregarded, and (ii) changes in free surface width caused by increasing and decreasing tidal levels or river discharge.

Comparison of Saline Water Intrusion

Figure 6 shows the intrusion length of the S/S_0=0.5 salt water isohaline with and without consideration of the diurnal inequalities on September 14, October 24, and November 29, 1978. In this figure, L_{st} and L_{sa} are the intrusion lengths with and without considering the diurnal inequalities, respectively.

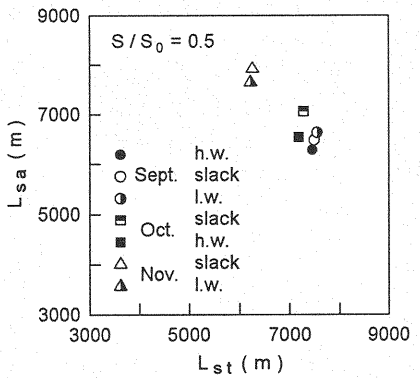

Figure 6 Intrusion length of salt water with and without diurnal inequality

With the diurnal inequality taken into consideration, salt water intrudes further upstream than when it is not considered in September and October, while in November the opposite results are obtained.

We investigate these two different results by considering an idealized tide, as shown Figure 7. The values of tidal displacement, which are integrated over t_0-t_1, t_1-t_2 and t_2-t_3, are set to A_1, A_2, and A_3, respectively and a parameter denoting the diurnal inequality is defined by the following equation. In cases where the diurnal inequality is not considered, P_t is equal to 1.

$$P_t = 2A_2/(A_1 + A_3) \tag{17}$$

P_t values averaged over the simulated period are 1.5 and 1.35 for September and October, respectively. On the other hand, in November, P_t is 0.85. These results suggest that positive tidal displacements from the mean sea level are large in comparison to the cases where the diurnal inequality is not considered in September and October. However, the opposite results are obtained in November. Predicting the intrusion length without considering the diurnal inequality, the intrusion length is underestimated for P_t>1. Meanwhile, the opposite result is obtained for P_t<1.

If a pumping station were to be constructed for river water, the diurnal inequality should be considered in a simulation and then it is necessary to carefully examine the mixing behavior of fresh and saline water.

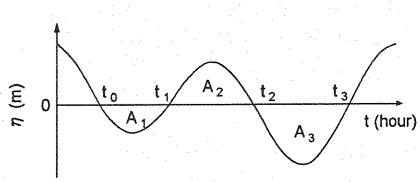

Figure 7 Idealized tidal response defining the diurnal inequality parameter

Effect of River Discharge on Saline Water Intrusion

Figure 8 shows how river discharge affects density current behavior. The simulation is carried out with respect to the tidal range during the period September 8-14, 1978. The river discharge is 4.4, 100,

and 500 m^3/s and the figures are for the high water phase.

Figure8(a) shows the result for a 4.4 m^3/s river discharge, which is less than the 9.4 m^3/s of Fig.4.(a). Contours of S/S_0=0.01, 0.025, and 0.05 intrude upstream after the shoal to approximately 9.5 km. For contours S/S_0=0.01 and 0.5, the salinity at the free surface is 0.32 and 0.17 times the salinity at the bottom.

Figure8(b) shows the result for a 100 m^3/s river discharge. In comparison with Fig.8(a), the salt water has retreated considerably downstream as a result of the greater river discharge. The contours S/S_0=0.01 and 0.05 are close together as in Fig.6(a). For a 500 m^3/s river discharge, the intrusion of salt water is halted near the river mouth by the large river discharge. The isohalines are denser than those in Figures 6(a) and (b).

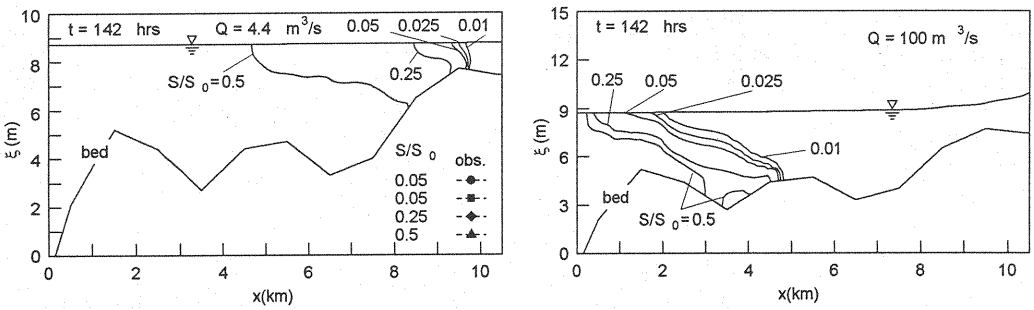

(a) Q =4.4 m^3/s (b) Q =100 m^3/s

Figure 8 Effect of river discharge on saline water intrusion

Figure 9 shows the intrusion length of the S/S_0=0.5 isohaline against river discharge at the high and low water phases. The intrusion length considerably decreases for river discharge rates between 100 and 200 m^3/s. When the river discharge exceeds 1,000 m^3/s, the intrusion of salt water almost completely stops. The intrusion distance almost uniquely depends on river discharge for a given tidal amplitude.

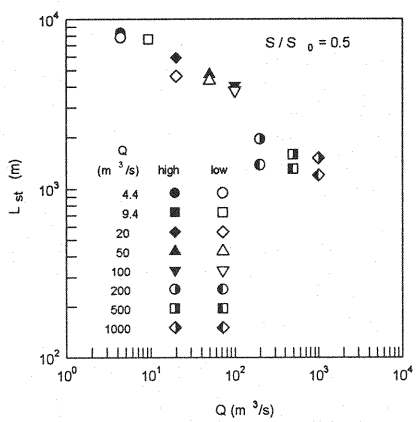

Figure 9 Intrusion length of salt water against river discharge

CONCLUSIONS

In this investigation, numerical simulations of salt water intrusion are conducted and the simulated results approximately satisfy experimental and observed behavior. However, the simulated results do not sufficiently explain the actual phenomena observed on site because, for example, lateral topography

changes are not considered. It is necessary to simulate actual density current behavior using a three-dimensional numerical model.

AKNOWLEDGEMENT

This study was supported by the Science Research Fund of the Ministry of Education (Representative: Hitoshi Tanaka, Tohoku University). Valuable data such as river discharge rates were provided by the Ministry of Construction, Shikoku region Construction Bureau, Ozu construction office.

REFERENCES

1. Bear J. : Hydraulics of Groundwater, McGraw-Hill, pp.225-239, 1979.
2. Ifuku, M. : Studies on salt wedge - Observations in Hiji river -, Memoirs of Ehime University, Sect.3 (Engineering),Vol.4, No.4, pp.313-331, 1978.
3. Ifuku, M. and Y.Kusu : Numerical analysis of saline intrusion with propagation of tide, Journal of Hydroscience and Hydraulic Engineering, Vol.17, No.1, pp.131-141, 1999.
4. Perrels, P.A.J. and M.Karelse : A two-dimensional numerical model for salt intrusion in estuaries, in: J.C.J.Nihoul (editor), Hydrodynamics of Estuaries and Fjords, Elsevier Scientific Publishing Company, pp.107-125, 1978.
5. Smagorinsky, J. : General circulation experiments with primitive equations, Month. Weather Rev., Vol.9, No.3, pp.99-164, 1963.

APPENDIX - NOTATION

The following symbols are used in this papaer:

a = tidal amplitude;
a_T, a_L = characteristic lengths defined by Eq.9;
B = channel width;
c_1 = empirical constant;
c_s = Smagorinsky constant;
g = gravitational acceleration;
h = still water depth;
K_{xx}, K_{zz} = longitudinal and vertical turbulent diffusivities, respectively;
L_{st}, L_{sa} = intrusion length with and without considering diurnal inequality, respectively;
p = pressure;
P_t = parameter of diurnal inequality;
Q = river discharge;
S = salinity;
S_0 = salinity of the sea;
S' = weighting coefficient;
t = time;
T = tidal period;
u, w = longitudinal and vertical velocities, respectively;
u_ξ = longitudinal velocity at the water surface;
x, z = longitudinal and vertical coordinates, respectively;
z_b = z-coordinate of the bottom;
γ_x, γ_z = constants of proportionality;
Δx, Δz = longitudinal and vertical grid intervals, respectively;
η = surface elevation;
ν, ν_t = kinematic viscosity and SGS diffusivity;
ξ = position of the free water surface;
ρ = fluid density
ρ_0, ρ_s = density of reference water and saline water, respectively;
σ = angular frequency; and
τ_{xx}, τ_{zx} = Reynolds stresses.

(Received August 22, 2000 ; revised December 22, 2000)